4
Bearing Fault Diagnosis

4.1 INTRODUCTION

Bearing faults are the major contributor of faults with 40-50% [Group et al., 1987] share in total motor faults. A typical ball bearing (shown in Figure 4.1(a)) can have defects in its outer race, inner race, cage and balls. Thus, the bearing faults are categorized as: 1. Outer Race Fault, 2. Inner Race Fault, 3. Cage Fault, and 4. Ball Defect. Bearing defects induce vibrations in the machines, therefore causing predictable frequencies in the vibration spectrum. These vibrations affect the air-gap eccentricities which perturb flux density. Consequently, there are modulations in the stator current; which can be observed in the stator current spectrum. As shown by [Schoen et al., 1995a], the vibration and current frequencies can be related by the following equation,

$$f_{bng} = |f_e \pm m.f_{bea}|, m = 1,2,3... \tag{4.1}$$

where, f_e is the supply frequency ($\frac{1440}{60} = 24Hz$), f_{bng} and f_{bea} are the characteristic fault frequencies in current and vibration spectrum respectively. The expressions of f_{bea} for various defects are given by following equations:

$$f_o = \frac{n}{2} f_{rm}\left(1 - \frac{BD}{PD}cos\phi\right) \tag{4.2}$$

$$f_c = \frac{1}{2} f_{rm}\left(1 - \frac{BD}{PD}cos\phi\right) \tag{4.3}$$

$$f_b = \frac{1}{2}\frac{PD}{BD} f_{rm}\left(1 - \left(\frac{BD}{PD}cos\phi\right)^2\right) \tag{4.4}$$

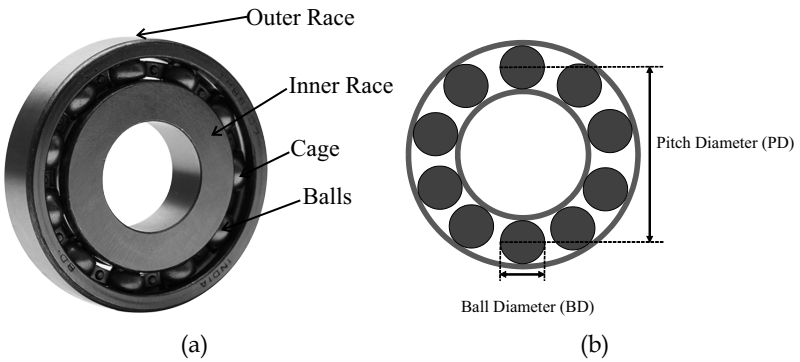

Figure 4.1 : (a) A typical ball-bearing and (b) its schematic diagram

Table 4.1 : Dimensions of the ball bearings under consideration

Bearing dimensions	Type 6205	Type 6204
Pitch Diameter (PD)	38.5 mm	33.5 mm
Ball Diameter (BD)	7.938 mm	7.938 mm
Number of balls (n)	9	8
Basic static load rating	7.8 kN	6.5 kN
Basic dynamic load rating	14.8 kN	13.5 kN

Table 4.2 : Fault frequencies of a ball bearing with f_{rm}=24 Hz and ϕ=0°

Type of fault frequency	Fault frequency in vibration spectrum (Hz)	Fault frequency in current spectrum (Hz) (for m=1)
6205		
f_o	85.732	35.73, 135.73
f_c	9.525	40.47, 59.53
f_c	130.267	180.267, 80.267
f_b	111.45	61.45, 161.45
6204		
f_o	73.252	123.25, 23.25
f_c	9.1365	40.84, 59.16
f_c	118.747	168.747, 68.747
f_b	95.98	45.60, 145.60

$$f_i = \frac{1}{2}\frac{PD}{BD} f_{rm}\left(1 + \left(\frac{BD}{PD}cos\phi\right)^2\right) \tag{4.5}$$

where, f_{rm} is the mechanical rotor speed, f_o, f_c, f_i and f_b are the fault frequencies for outer-race, cage, inner-race and ball faults respectively, PD is the pitch diameter, BD is the ball diameter, n is the number of balls in the bearing and ϕ is the contact angles for the ball on races (in radians). The schematic diagram of a ball bearing is shown in Figure 4.1(b).

With the help of dimensions of the bearing, the fault frequencies of various bearing faults can be calculated. The dimensions of the ball bearing taken into consideration in the present study (Type 6205 and Type 6204) are presented in Table 4.1. Thus, the fault frequencies for all four types of bearing faults can be computed using Equations 4.2-4.4 and are provided in Table 4.2. These frequencies are used to analyse the signatures of the bearing faults for their detection, location and classification.

4.2 FAULT DETECTION

In this section, two methods for detection of bearing faults have been proposed. One is based on Stockwell transform and other is based on the Total Harmonic Distortion. The details of each fault detection method are given as follows:

4.2.1 Stockwell transform based fault detection

The fault detection is performed using ST matrix. The analysis involves current acquisition of a three-phase induction motor with various bearing conditions. Subsequently, the current signals are transformed to time-frequency plane using ST and further the resultant complex matrix is analysed to identify fault signatures. The details are explained in the following paragraphs:

Experimental set-up

The experimental-set up used has a three-phase four-pole induction motor ratings 3.0 HP, 415 V, 4.5 A, 1440 rpm. The rotor of the motor is mounted on two ball bearings with Type 6205 on driving-end and Type 6204 on fan-end. The three-phase current signals were recorded using Yokogawa WT3000 Power Network Analyzer. These current signals were sampled at 5.0 kHz i.e., 100 samples per cycle. Figure 4.2 shows the picture of experimental set up for recording stator current signals of the induction motor. The bearings with various defects used for the experimental study are shown in Figure 4.3. Initially the motor was run with healthy bearings on both the ends in order to obtain reference features which would be utilized for detection and further diagnosis. Later, the bearings with various defects were mounted on driving-end (Figure 4.3(a)) keeping healthy bearing on the fan-end. In order to study the effect of defective bearing position on fan-end (Figure 4.3(b)), the bearing of same defects are used on the fan-end keeping healthy bearings at the driving-end.

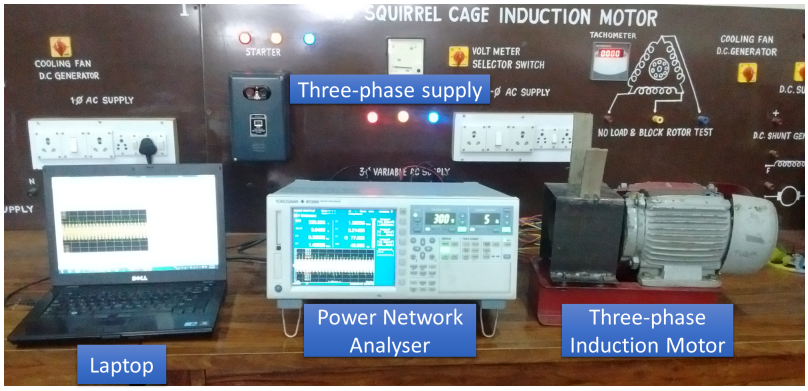

Figure 4.2 : Experimental set up for recording of current signals with bearing faults in a three-phase induction motor

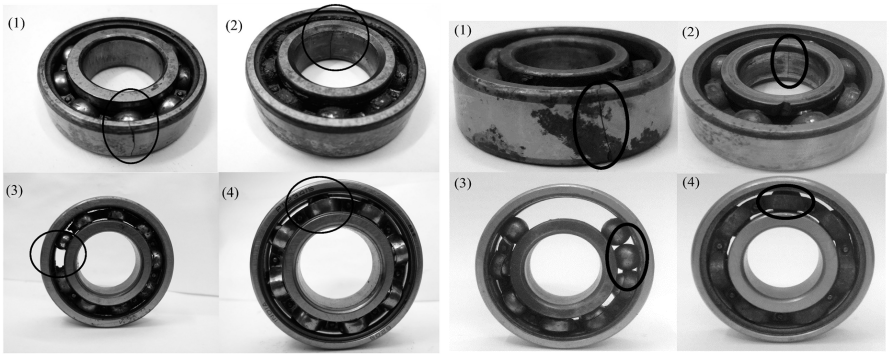

Figure 4.3 : Set of the bearings with fault in (1) outer-race, (2) inner-race, (3) cage and, (4) ball, at (a) driving-end, (b) fan-end

Methodology

The proposed methodology to diagnose bearing faults with the help of Stockwell Transform is explained in Figure 4.4. The recorded signals are analysed using Stockwell transform to obtain complex ST-matrix, $S(f,t)$. The maximum magnitude $A_{max} = max(|\ S(f,t)\ |)$ and maximum phase $\Theta_{max} = max(\angle S(f,t))$ matrices are obtained from this ST-matrix.

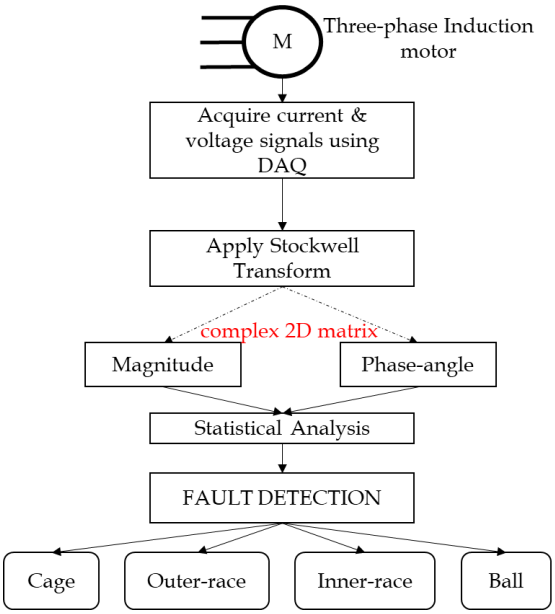

Figure 4.4 : Block diagram of the proposed methodology for analysis of bearing faults

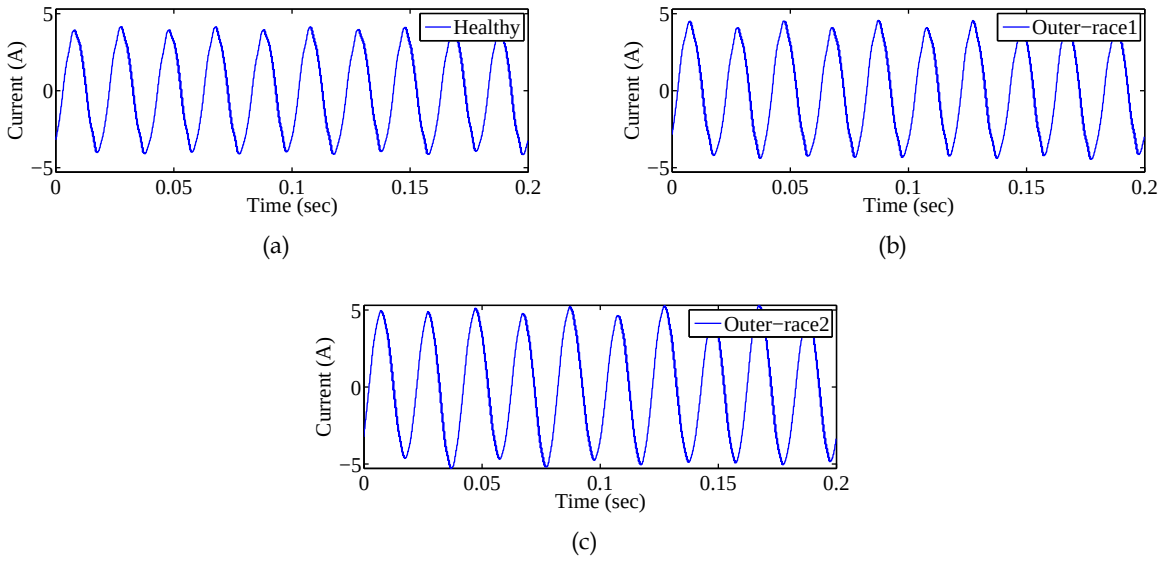

Figure 4.5 : Current signals for various bearing cases where outer-race1 at driving-end and outer-race2 at fan-end

Various statistical properties such as maximum, minimum, mean, mode, standard deviation and variance of these magnitude and phase angle of ST matrix were analysed in the viewpoint of fault detection. Out of these properties, the standard deviation of these matrices were found to be effective in the detection and analysis of various bearing faults.

The stator current signals recorded at 5 kHz sampling frequency are shown in Figure 4.5 for the driving-end bearing samples. They are decomposed using Stockwell-transform, to obtain ST matrix for various bearing defects whose contour plots are as shown in Figure 4.6 and Figure 4.7 for the defective bearings mounted at driving-end and fan-end respectively. From these figures, it can

be observed that the various bearing defects possess different densities in highlighted areas. Thus these contours help in detecting bearing faults and analysing them. For this purpose the maximum magnitude and the maximum phase angle plots are obtained and analysed in the domain of statistics.

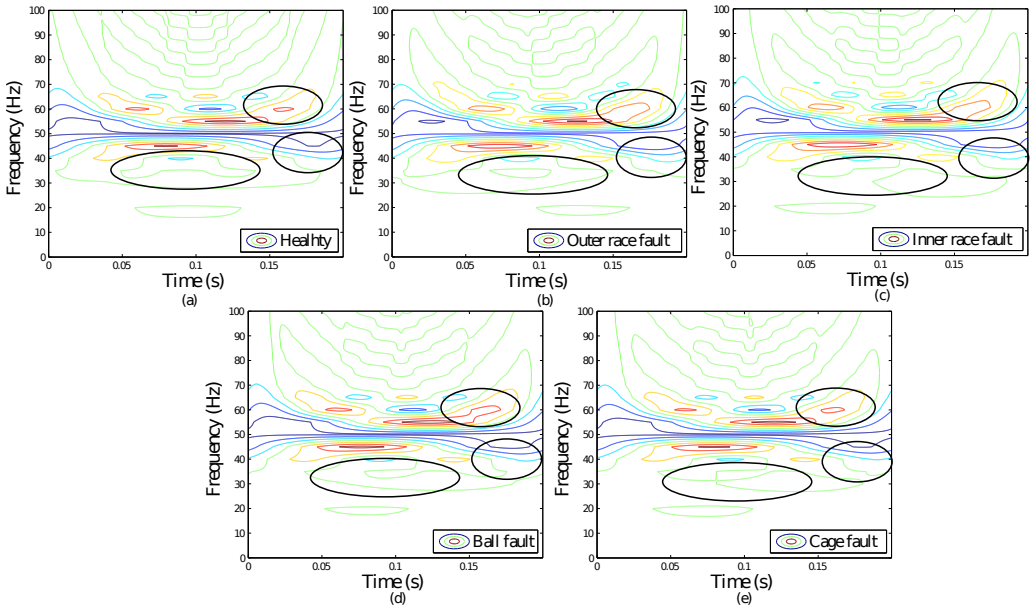

Figure 4.6 : Contours based on S-transform for various bearings conditions on driving-end. Highlighted areas depict differences in density of contour plot in various cases.

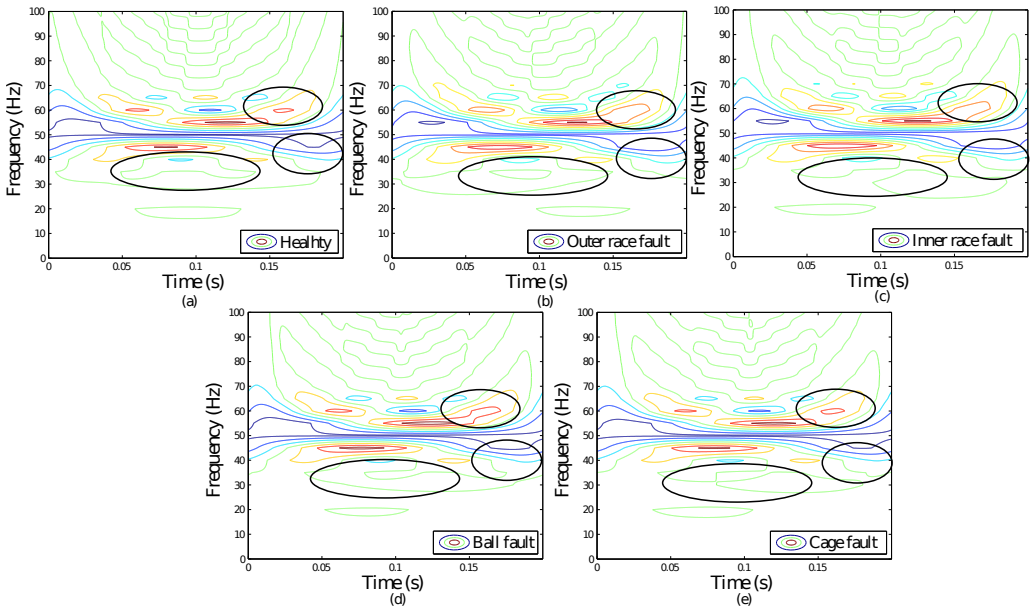

Figure 4.7 : Contours based on S-transform for various bearings conditions on fan-end. Highlighted areas depict differences in density of contour plot in various cases.

Results and Discussion

The maximum magnitude plots in Figure 4.8(a) present a clear discrimination among various bearing conditions whereas the maximum phase plot in Figure 4.8(b) fails to provide

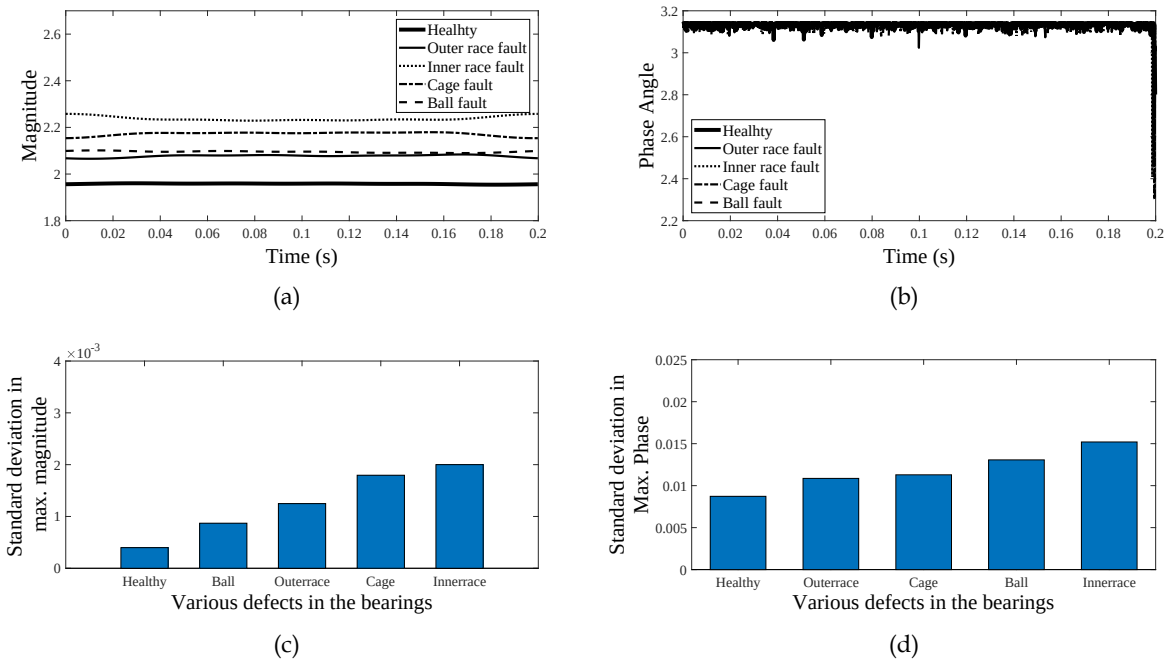

Figure 4.8 : (a) Maximum magnitude plot, (b) Maximum phase angle plot; Standard deviation for (c) Max. magnitude and (d) Max. phase plots for various bearing conditions on driving-end.

such discrimination. However, the standard deviation computed for maximum magnitude and maximum phase angle vectors as shown in Figure 4.8(c) and 4.8(d) provide a discrimination among various bearing conditions. It is also evident that the healthy bearings possess minimum standard deviation and various bearing defects are characterized by different values of the same.

Figure 4.9(a) and Figure 4.9(b) present the maximum magnitude and maximum phase angle plots for various bearings conditions on fan-end respectively. The maximum magnitude plots in Figure 4.9(a) provide a discrimination among various bearing conditions. But the maximum phase angle plots fail to do the same as evident from Figure 4.9(b). However, the standard deviation computed for maximum magnitude and phase angle vectors help in discriminating various bearing conditions as shown in Figure 4.9(c) and Figure 4.9(d).

From Figure 4.8(c) and 4.8(d), Figure 4.9(c) and 4.9(d), it is evident that the maximum magnitude values associated with fan-end bearing defects have higher values compared to those associated with driving-end bearing defects. It can also be observed that the standard deviation values of maximum phase angle for the defective bearings on fan-end are higher in comparison with defective bearings on driving-end.

These observations could be supported by the fact that damping caused due to loading, suppress the vibrations induced by defective bearings at shaft-end while such loading could not provide sufficient damping to the vibrations caused by bearing defects at fan-end [Schoen et al., 1995a]. Hence, the standard deviation associated with fan-end defective bearings are bound to have large values.

In this method, the features extracted from the ST matrix of the Stockwell-transform can be effectively utilized for the detection and analysis of various bearing faults. The standard deviation of maximum magnitude and maximum phase angle vectors help in discriminating different bearing conditions. Healthy bearings are characterized by minimum standard deviation

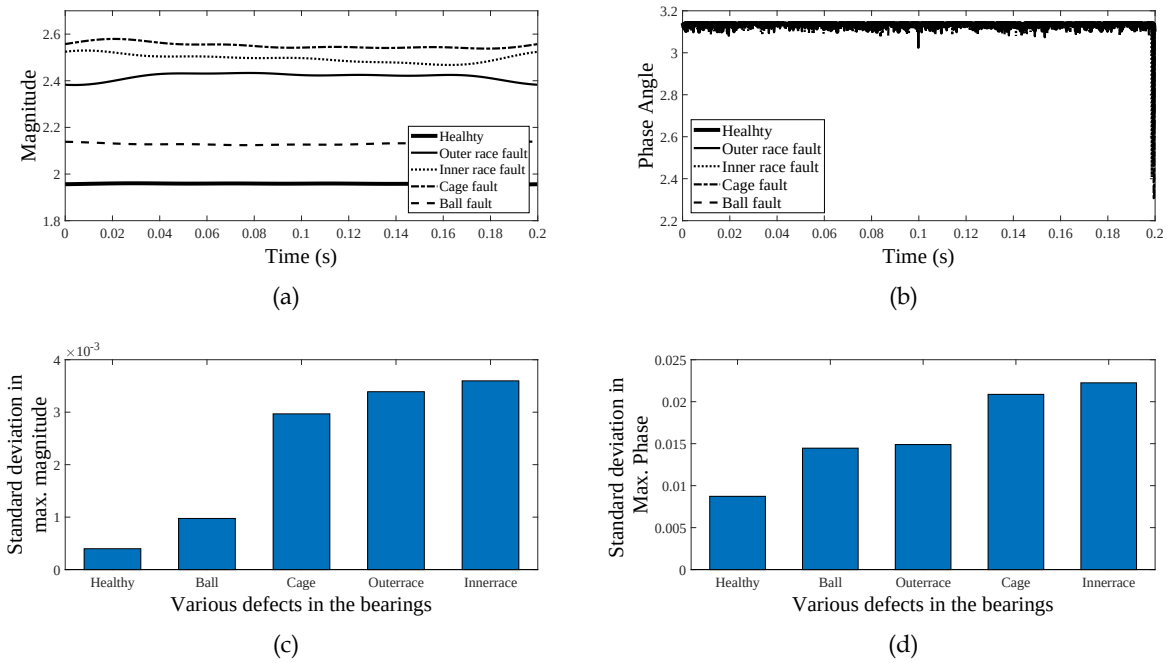

Figure 4.9 : (a) Maximum magnitude plot and (b) Maximum phase angle plot;Standard deviation for (c) Max. magnitude and (d) Max. phase plots for various bearing conditions on fan-end.

values whereas different higher values characterize various defects. The standard deviations for fan-end bearing defects are found to be higher than those obtained for driving-end bearing defects.

4.2.2 Total Harmonic Distortion based fault detection

In the proposed fault detection method, the stator currents of a three-phase induction motor are analysed with the Fast Fourier Transform. The Total Harmonic Distortion (THD) for voltage and current signals are computed using FFT.

Methodology

A fault index given by the following relation is calculated and compared with a threshold value which is nothing but the fault index of healthy bearing. If the fault index is greater than the threshold then the bearing is identified as defective bearing. The fault index (FI) is defined as:

$$FI = THD(current) - THD(voltage) \tag{4.6}$$

Using this fault index, a threshold can be defined such that healthy would be low from this threshold, while faults would have higher fault index. The experimental set-up used and the results are described below:

Experimental Set-up

The experimental set-up comprises a 3HP, 3-phase, 4-pole, 440 V, 50 Hz induction motor whose rotor is supported by two bearings, Type 6204 (fan-end) and Type 6205 (driving-end) as shown in Figure 4.10. The data acquisition system includes *NI cDAQ9178* chassis, *NI 9247* current module (50 Amp), *NI 9225* voltage module and an interfacing software *LabView 2012*. The defective bearings collected from the industry are batched into three categories i.e. bearings with ball fault, cage fault and outer-race fault as shown in Figure 4.11 for fan-end and driving-end. Each batch has

14 number of bearings per category. Thus a total of 42 defective bearings belonging to different conditions are used for the study. Apart from these defective bearings, experiment has been conducted with a set of new bearings also. A total of 49 case studies have been conducted with the variations in the type of defect and location of each bearing defect. In each case, the three-phase stator current signals are sampled at 6.4 kHz with 128 samples per cycle.

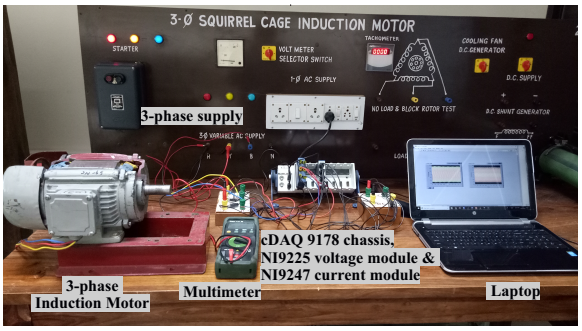

Figure 4.10 : Experimental set up for the measurement of current signals of induction motor under normal and faulty conditions.

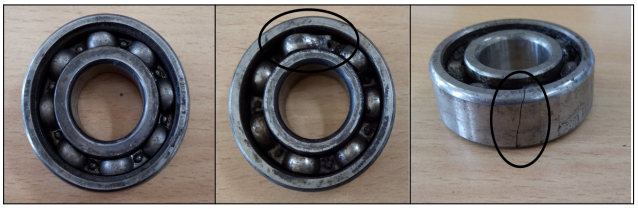

(a)

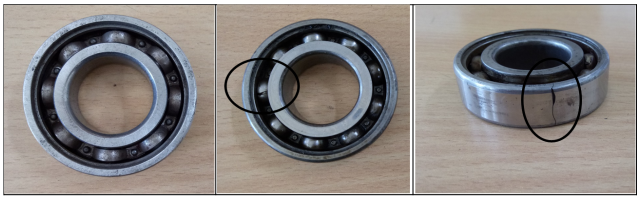

(b)

Figure 4.11 : Bearings of Type (a) 6204 and (b) 6205 with (1) ball fault, (2) cage fault, and (2) outer-race fault

Results and Discussion

The Fourier Transform of supply voltage and stator current signals (for healthy and bearing with ball defect) are presented in Figure 4.12(a) and 4.12(b) respectively.

Based on these FFT plots, fault indices are calculated. Figure 4.13(a) depicts the fault index FI computed for fault detection for healthy and bearing with ball fault. From this figure, it is evident that the fault index FI for ball fault is higher than that of a healthy bearing. Figure 4.13(b) illustrates fault indexes of ball, cage and outer-race faults along with those of the healthy bearings. It can also be observed that all types of faults have fault index greater than the fault index of a healthy bearing. Thus a threshold value of 0.0041 can be selected to discriminate defective bearing from the healthy bearings.

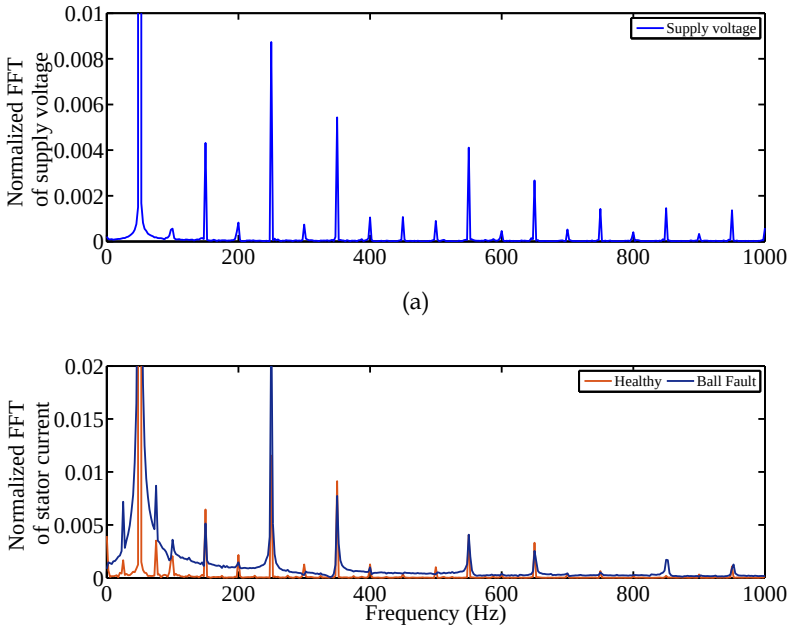

Figure 4.12 : FFT of (a) Supply voltage and (b) current signals (healthy and ball fault).

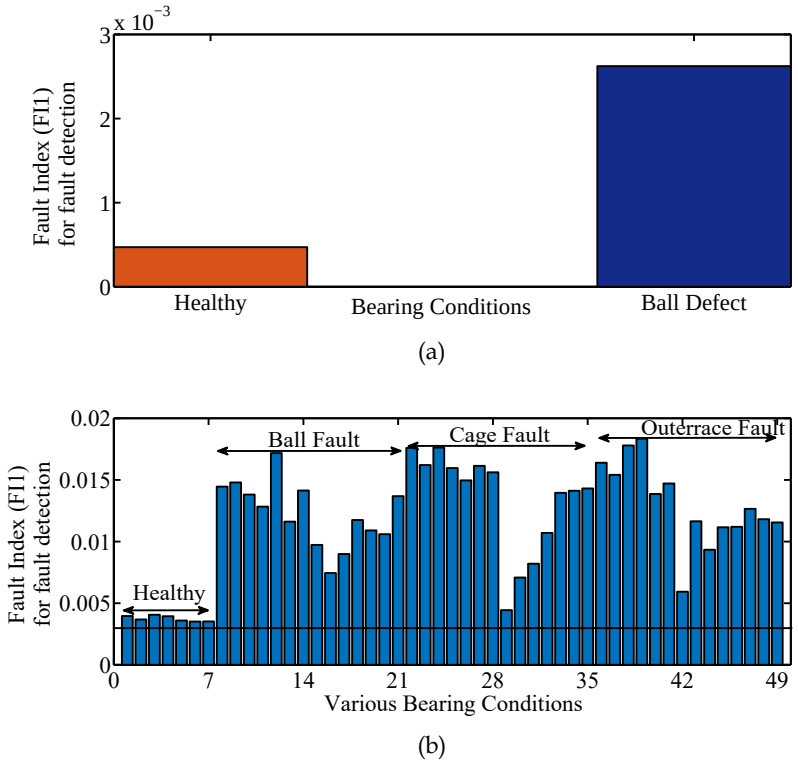

Figure 4.13 : Fault index (FI) for (a) healthy and ball fault and (b) all bearing conditions

4.3 LOCATION OF FAULTY BEARING

The fault detected and classified may be present in either fan-end bearing or driving-end bearing. Thus, it is important to identify the defective bearing such that it can alone be replaced. In this case study, location of the faulty bearing i.e., driving-end or fan-end has been investigated with the help of Stockwell transform and Support vector machine. In the literature, the detection and classification of bearing faults have been reported under various case studies. However, identifying the location of a bearing fault is also a major problem. The knowledge of location would lead to reduction in maintenance and cost since it would not involve unnecessary dismantling of motor.

There are two methods suggested for locating the faulty bearing. First method is based on decomposing current signals using Stockwell transform, followed by feature extraction and then feature reduction technique with Principal Component Analysis (PCA), followed by classification using Support Vector Machine (SVM). In the second method, the location is determined with the help of features from ST matrix. The details are described below:

4.3.1 Location based on Stockwell transform and SVM

In this work, an effort has been made to locate the defective bearing using features extracted from ST on which PCA is applied to reduce the dimensions. The resultant high-variance components are fed to SVM to classify the samples on the basis of their locations. In the following sub-sections, methodology of the proposed detection of location is explained in detail, followed by experimental set-up details and then the results.

Methodology

The current signals are recorded from the experimental set-up for different bearing samples. With the help of Stockwell transform, the signals are decomposed into magnitude and phase angle of ST matrix. Features are extracted from these matrices to form a feature matrix of the samples. PCA is used to reduce the dimension of the feature matrix. The components giving more than 90% variance in the data are chosen to feed SVM classifier. With these input features, SVM is trained and tested using *k*-fold cross validation with RBF kernel. The detailed steps are explained below:

Feature Extraction and PCA

The stator current signals are analysed with Stockwell Transform (ST) which results in a ST matrix. This complex two-dimensional matrix (in time-frequency plane) can be split into magnitude and phase angle for further analysis. The statistical properties such as mean, maximum, standard deviation and kurtosis of these matrices are calculated along time and frequency axes to form statistical vectors which will be 16 in number. The length of each vector along time axis is equal to the number of samples collected over two cycles. Similarly, the vector along frequency axis has a length depending on the chosen frequency range. These statistical vectors are presented in Table 4.3. Further, properties such as mean, maximum and standard deviation are computed for these statistical vectors which give rise to 16*3 = 48 features.

To extract most significant features, Principal Component Analysis (PCA) is used to extract the principal components of the obtained feature vector. On the basis of cumulative variance of components, the significant principal components are chosen such that they capture more than 90% variability of the data. These selected components are fed to SVM as input features to first train and then identify the locations of the test defective bearings.

Location of Defective Bearing with SVM classifier

SVM is utilized to predict the location of pre-determined faults from two locations. SVM is fed

Table 4.3 : Statistical Properties of Magnitude and Phase Angle of ST matrix

S.no	Statistical Vectors of ST Matrix
1	Maximum of Magnitude on time axis
2	Standard deviation Magnitude on time axis
3	Kurtosis of Magnitude on time axis
4	Mean of Magnitude on time axis
5	Maximum of Magnitude on freq. axis
6	Standard deviation Magnitude on freq. axis
7	Kurtosis of Magnitude on freq. axis
8	Mean of Magnitude on freq. axis
9	Maximum of Phase Angle on time axis
10	Standard deviation of Phase Angle on time axis
11	Kurtosis of Phase Angle on time axis
12	Mean of Phase Angle on time axis
13	Maximum of Phase Angle on freq. axis
14	Standard deviation Phase Angle on time axis
15	Kurtosis of Phase Angle on freq. axis
16	Mean of Phase Angle on freq. axis

with input features of both locations in its training phase and later the trained model is utilized to predict location of fault for test data. Radial Basis function has been popularly used as the kernel function for SVM. The parameters such as cost parameter (C) and gamma parameter (γ) are found using k-fold cross-validation method. Using varied values of C and γ, optimal values are found using cross validation with $k = 4$. The training set with chosen components are used as input to train the SVM. The steps of the proposed strategy are detailed in the flowchart shown in Figure 4.14.

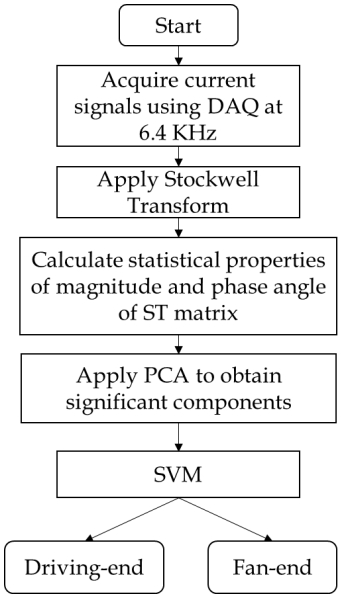

Figure 4.14 : Flowchart of the proposed algorithm for detecting the location of faulty bearings

Experimental Set-up

The experimental set-up described in Section 4.2.2 has been used. In this case, two types of faults are taken into consideration, ball fault and outer-race fault, whose prototypes are shown in

Figure 4.15. There are 14 set of bearings with ball fault located at driving-end and fan-end locations (i.e, 7 on each end of the motor). Similarly, 14 set of bearings with outer-race fault at both locations. Thus, a total of 28 faulty bearings are used for this study, out of which 14 bearings belong to fan-end and remaining 14 belong to driving-end.

(a) (b)

Figure 4.15 : Bearings with Fault-1: Ball fault and Fault-2: Outerrace fault at (a) fan-end and (b) driving-end of the motor

Results and Discussion

The stator current signals acquired from DAQ system are shown in Figure 4.16. The stator

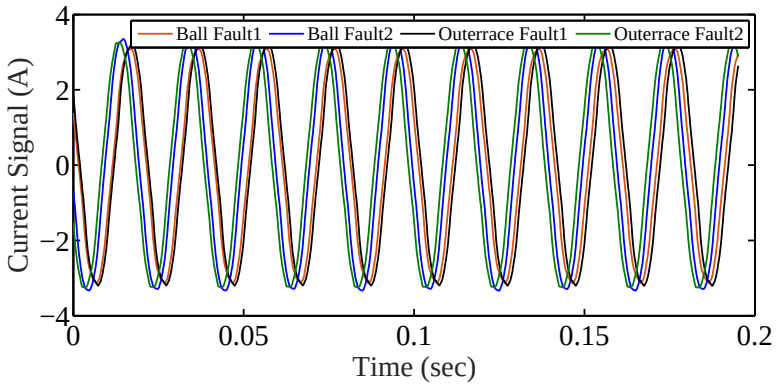

Figure 4.16 : Current signals of bearings with ball fault and outerrace fault present at either fan-end or driving-end

current signals are decomposed using Stockwell transform to obtain ST matrix for each bearing condition. The statistical vectors are computed for two cycles over for a fixed frequency range. According to Table 4.1, the frequency range for both ball and outer-race fault can be chosen by observing their minimum and maximum frequencies, which gives us the range as [20 Hz - 160 Hz]. Among these statistical features, standard deviation (SD) of the maximum magnitude matrix with respect to time and frequency axis are shown in Figure 4.17 and Figure 4.18 for illustration purpose. Figure 4.17(a) and 4.17(b) show SD of magnitude with respect to time and frequency axis respectively and Figure 4.18(a) and 4.18(b) show SD of phase angle with respect to time and frequency axis respectively. It is evident from Figure 4.17(a) that fan-end located faults have significantly different values than driving-end located faults. Figure 4.17(b) and 4.18 show similar variations between faults at two locations. Other statistical properties were also found to be significantly varying under different fault locations. Therefore, these features are collectively utilized to form a feature vector for each fault case at two locations.

The 48 features extracted from the experiment conducted with each defective bearing are analysed with PCA to extract the uncorrelated principal components. The variance and cumulative variance of principal components are shown in Figure 4.19(a) and 4.19(b) respectively. It can be observed that more than 90% of the variance is captured in first 9 components. Hence, these 9

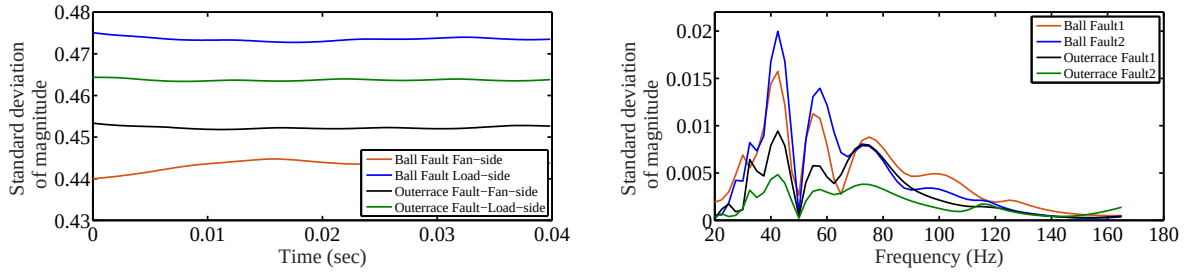

(a) (b)

Figure 4.17 : Standard deviation of magnitude of ST matrix with respect to (a) time and (b) frequency axis

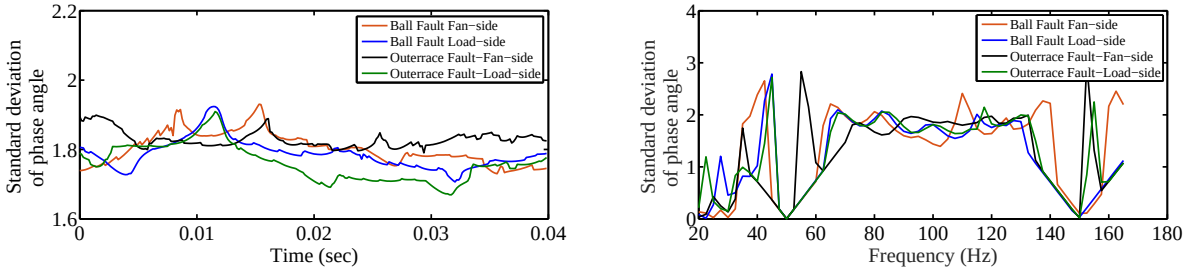

(a) (b)

Figure 4.18 : Standard deviation of phase angle of ST matrix with respect to (a) time and (b) frequency axis

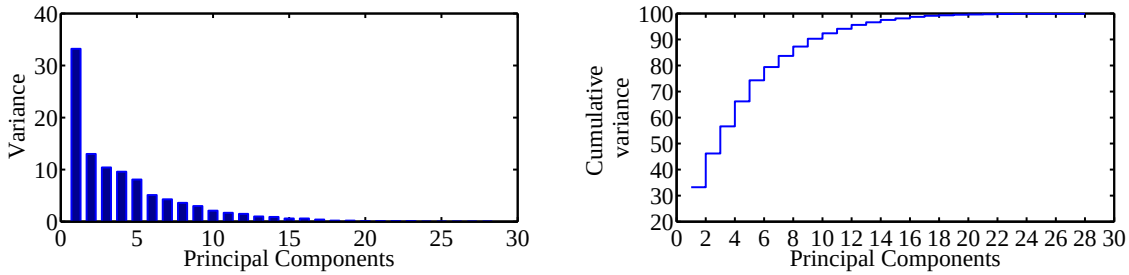

(a) (b)

Figure 4.19 : (a) Variance of each component extracted by PCA, (b) their cumulative variance

components can be used to represent original feature vector and thereby used for further analysis. The scatter plots shown in Figure 4.20 illustrates that the selected principal components have clear boundaries and hence can be efficient inputs to SVM classifier.

The 9 components are used as final features to be fed to SVM. Out of 14 bearings of each fault type, 8 bearings (4 of each end of the motor) are used as training and remaining 6 (3 of each end) are used for testing. Thus, training set comprises of 16 bearings dataset while testing set has 12 bearings dataset. Radial basis function (RBF) has been used as the kernel function for SVM. The optimal values of cost (C) and gamma parameter (γ) are found using 4-fold cross validation. For

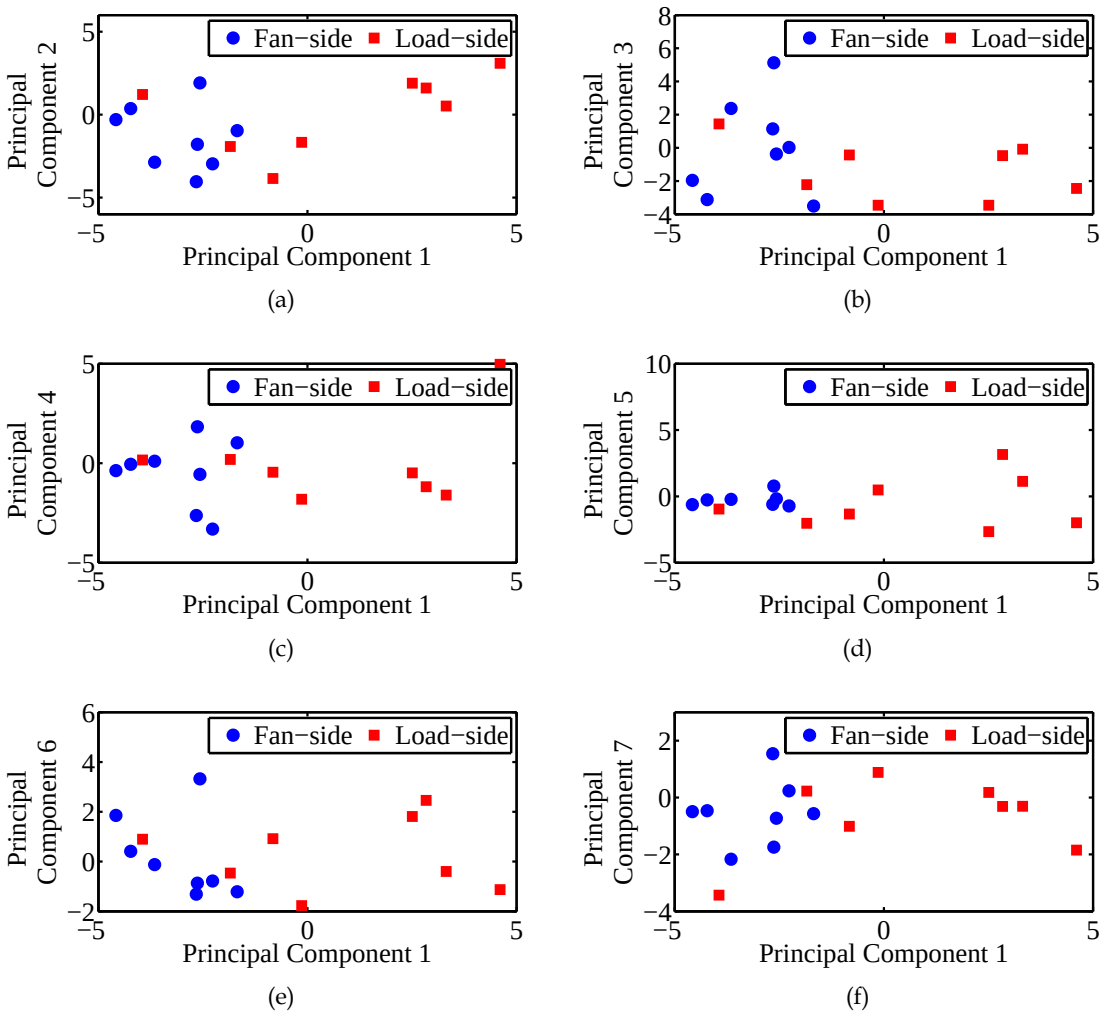

Figure 4.20 : Scatter plot of training set using Principal Component 1 against other Principal Components

this purpose training dataset has been used and the values of C and γ with which best classification performance achieved, are selected as optimal values. The obtained values in logarithmic bases of C and γ are 31.5 and -7.75. With these values of parameters, the trained model is tested with the test data and the results are shown in Table 4.4. The accuracy of correctly locating the defective bearing is achieved to be 91.667%.

Table 4.4 : Location of defective bearing with SVM

Class	Total Samples	Correctly Identified	Misidentified
Fan-end	6	5	1
Driving-end	6	6	0

Thus, defective bearings in a three-phase induction motor can be effectively located by analysing the stator currents with the help of Stockwell Transform. The features extracted from ST are analysed with PCA for the selection of non-redundant and relevant features. These features are fed to SVM to find whether the defective bearing is at either fan-end or driving-end. The performance of the proposed algorithm has been established by the experimental studies on

defective bearing collected from the industry. Thus, the proposed algorithm can be used for online condition monitoring of the bearing so as to minimize maintenance and/or downtime of the equipment used in the industry.

4.3.2 Location based on Stockwell transform

In this work, another method for locating the faulty bearing is proposed based on the features of ST matrix. The current signals are decomposed using ST which provides complex matrix which can be further decomposed into magnitude and phase angle matrices. Statistical features from these matrices are computed and amongst which some features are found to be effective for determining location. The proposed location detection method can be implemented only when the fault is known a priorly.

Methodology

The maximum of maximum magnitude (along the frequency axis) is found to be varying significantly depending upon defective bearing location in case of ball faults. Similarly, the maximum of maximum phase angle (along the frequency axis) is found to be varying significantly depending upon defective bearing location in case of cage and outer-race faults. Hence, these parameters are named as the fault indexes FI_1 and FI_2 as given below which will be compared with respective thresholds to locate defective bearing in case of ball faults and cage/outer-race faults respectively.

1. Ball Fault

$$FI1 = max(max(|S(\tau, f)|)) \tag{4.7}$$

2. Cage Fault and Outerrace Fault

$$FI2 = max(max(\phi(S(\tau, f)))) \tag{4.8}$$

Thus, for ball faults, one fault index $FI1$ is proposed and for other two faults, cage and outer-race faults, $FI2$

Experimental Set-up

The same experimental set-up as described in Section 4.2.2 has been used here. Same number of bearings were used. Once the type of fault is known, the following method can be used to identify the location.

Results and Discussion

The fault index ($FI2$) is calculated for bearings with ball faults are shown in Figure 4.21(a). From this figure, it can be seen that FI2 is smaller for fan end defective bearings compared with that of driving-end. Hence, a threshold of 1.5933 can be set for $FI2$ to locate whether the defective bearing is located either on fan-end and driving-end. Similarly, the fault index $FI3$ computed for bearings with cage and outer-race faults is shown in Figure 4.21(b) and 4.21(c) respectively. It can be observed that in case of cage faults, except two samples (which belong to driving-end), all samples have significantly larger values of $FI3$ as compared to fan-end faults. On the other hand, in outer-race faults, the load-end faults have larger values than fan-end faults. Thus, a threshold of 8.5e-15 can be set for $FI3$ to locate whether the defective bearing is located either on fan-end and driving-end for both cage and outer-race faults.

Thus, the location of defective bearing can be effectively be carried out with the help of fault

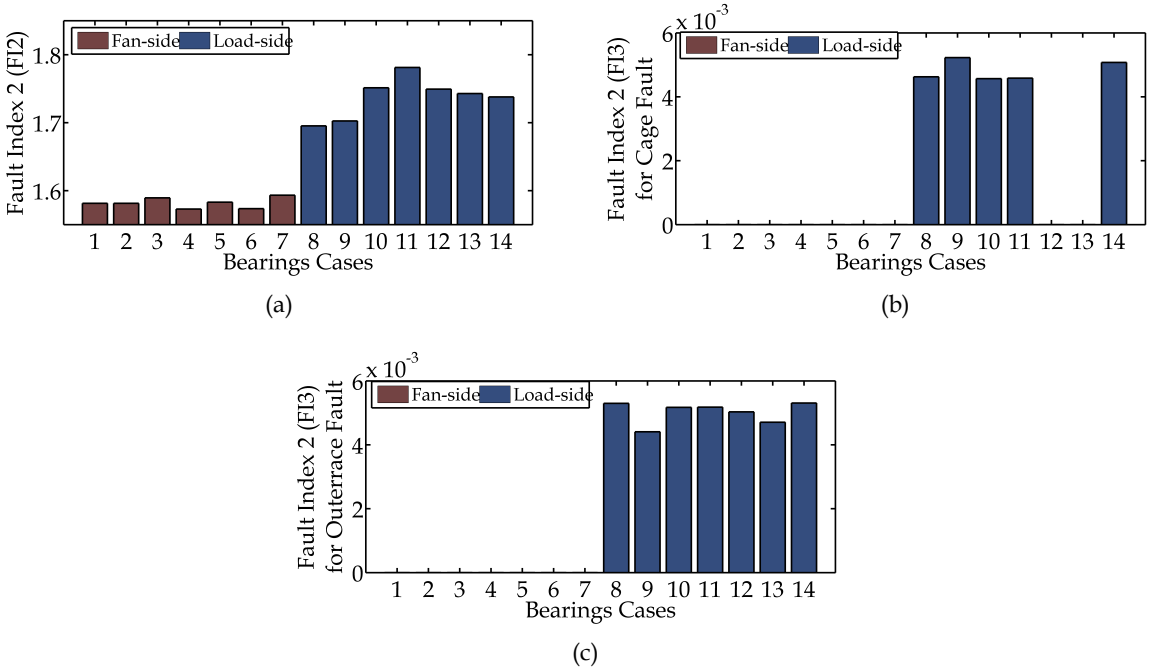

Figure 4.21 : Fault indexes to locate (a) ball fault, (b) cage fault, and (c) outer-race fault either at fan-end and driving-end.

indexes *FI*2 and *FI*3 by comparing with their respective threshold followed by fault classification. The accuracy of locating the defective bearing is given in Table 4.5.

Table 4.5 : Details of location identification

Fault Type	Correctly Identified	Misidentified	Accuracy
Ball Fault	14	0	100%
Cage Fault	12	2	85.7%
Outer-race Fault	14	0	100%

4.4 FAULT CLASSIFICATION

In this work, an algorithm has been proposed for classification of various bearing faults such as outer-race, cage and ball faults in a three-phase induction motor. For fault classification current signals are decomposed with Stockwell Transform and features are extracted. Feature selection is performed before feeding to the classifier. The same features are fed to ANN in order to establish the superiority of SVM over ANN in terms of classification efficiency.

Methodology

The current signals are analysed with ST to extract possible features based on statistical properties of phase and magnitude plots of the ST matrix. These features along with FFT of current signals are combined to form a feature matrix. These features are ranked by using Fisher Score algorithm. The correlation of these features is computed and compared with a pre-set threshold in order to select non-redundant features. These features are fed to SVM in order to finalize the feature selection with maximum possible accuracy. This methodology has following steps:

Stockwell Transform provides a complex matrix whose rows represent variation in time and columns represent variation in frequency. The statistical parameters such as maximum, mean, standard deviation and kurtosis of magnitude and phase angle of the ST matrix are computed along time and frequency axes. The analysis has been restricted to a specific range of 20 to 165 Hz as illustrated in Section A of Theoretical Background and the duration of signal considered is 2 electrical cycles (40 ms). Thus, the number of rows of the ST matrix becomes 59 on the frequency axis with the frequency resolution of 2.5 Hz and the number of columns become 256 (128 samples per cycle) leading to a size of 59x256. Consequently, each statistical parameter computed based on magnitude of ST matrix on frequency axis would give rise to a vector of length 256 whereas the same computed along time axis would lead to a feature vector of length 59. Eventually, each statistical parameter would yield a total of 315 (256 + 59) features. Similarly, each statistical parameter computed based on phase angle of ST matrix will yield another 315 (256 + 59) features. Thus for the four statistical parameters (maximum, mean, standard deviation and kurtosis) computed based on the magnitude and the phase angle would yield a total of 2520 (2x315x4) features. Apart from 2520 features extracted from ST matrix, the 59 magnitudes of each frequency component obtained from FFT are utilized to make a total of 2579 features. The statistical properties utilized for the extraction of these features are presented in Table 4.6.

Table 4.6 : Features for fault diagnosis

S.no.	Parameters of ST Matrix	Formula
1.	FFT of the current signal	$fft(x(t))$
2.	Maximum of Magnitude matrix	$max(S(\tau, f))$
3.	Mean of Magnitude matrix	mean$(S(\tau, f))$
4.	Std. dev of Magnitude matrix	std$(S(\tau, f))$
5.	Kurtosis of Magnitude matrix	kurtosis$(S(\tau, f))$
6.	Max of Phase matrix	max$(\angle S(\tau, f))$
7.	Mean of Phase matrix	mean$(\angle S(\tau, f))$
8.	Std. dev of Phase matrix	std$(\angle S(\tau, f))$
9.	Kurtosis of Phase matrix	kurtosis$(\angle S(\tau, f))$
10.	Maximum of Magnitude matrix on freq. axis	$max(\|S(\tau, f)\|)$
11.	Mean of Magnitude matrix on freq. axis	mean$(S(\tau, f))$
12.	Std. dev of Magnitude matrix on freq. axis	std$(S(\tau, f))$
13.	Kurtosis of Magnitude matrix on freq. axis	kurtosis$(S(\tau, f))$
14.	Max of Phase matrix on freq. axis	max$(\angle S(\tau, f))$
15.	Mean of Phase matrix on freq. axis	mean$(\angle S(\tau, f))$
16.	Std. dev of Phase matrix on freq. axis	std$(\angle S(\tau, f))$
17.	Kurtosis of Phase matrix on freq. axis	kurtosis$(\angle S(\tau, f))$

Fisher score criterion is used to order (or rank) the features based on the scores. These features are further shortlisted based on minimum correlation of 50%. The final selection of features fed to SVM are selected based on a maximum efficiency of classification as detailed below:
Step 1. Initialize the feature set with the top two ranked features.
Step 2. Compute the classification accuracy of the SVMs with the combination of features in Step 1.
Step 3. If the accuracy is less than 100%, add next ranked feature and update the possible combinations.
Step 4. Repeat Step 2 and 3 until all testing data is successfully classified or all features are exhausted.

Thus, the features which yield maximum accuracy are finalized as the features required by the SVMs for proposed fault diagnosis. Since the defects have to be classified into three categories using SVM i.e. ball fault, cage fault and outer-race fault, two SVMs namely SVM1 and SVM2 are proposed for this purpose. SVM1 separates ball fault from other faults (cage and outer-race fault)

and SVM2 separates cage fault and outer-race fault. The block diagram of fault diagnosis using two-stage SVM is shown in Figure 4.22.

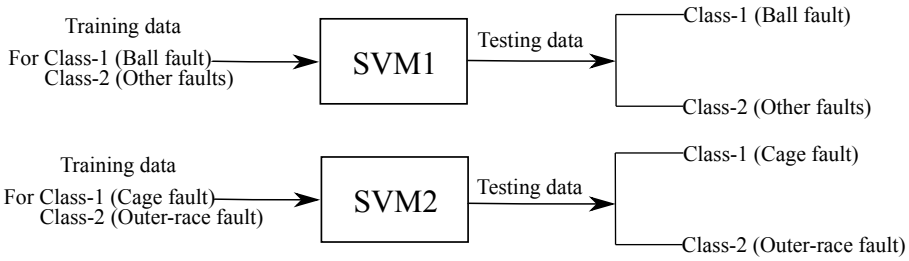

Figure 4.22 : Fault classification using OAA-SVM

Experimental Set-up

The same experimental set-up as described in Section 4.2.2 has been used. The number of bearings used for the experiments are kept same.

Results and Discussion

Features extracted from 42 bearings are divided into two databases. One database containing the features of 24 bearings (different conditions and locations) is utilized for training SVM1 and 16 bearings (different conditions and locations) are utilized for training SVM2. The second set of database used for testing are obtained from the experiments conducted on 18 bearings for SVM1 and 12 bearings for SVM2. SVM with various kernels such as linear, Gaussian, polynomial and sigmoid have been tried and found no significant differences in the performances. Hence, linear SVM is chosen because of its low computational burden and speed in convergence. The cost parameter (C) which sets soft margin in the classifier is chosen using 10-fold cross-validation. The training dataset has been used for cross-validation process. The values of C found to be 101 and 7.5 for SVM1 and SVM2 respectively.

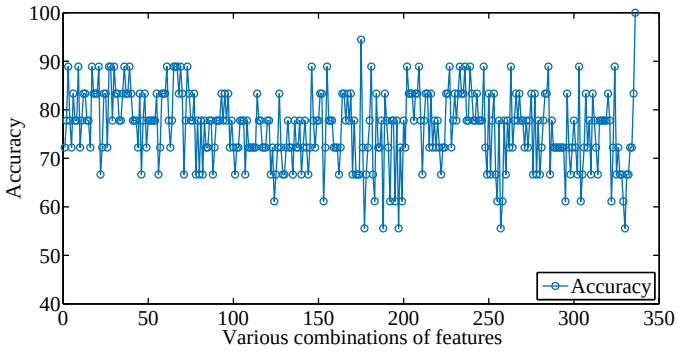

Figure 4.23 : Accuracy for various combinations of four features for classification of ball fault and other faults using SVM1

A classification accuracy of 100% is achieved by SVM1 with the four features detailed in Table 4.7 as per the proposed algorithm. Figure 4.23 represents the performance of different combinations of four features.

Similarly, a classification accuracy of 91.667% is achieved by SVM2 with two features described in Table 4.8 as per the proposed algorithm. The classification performance of various

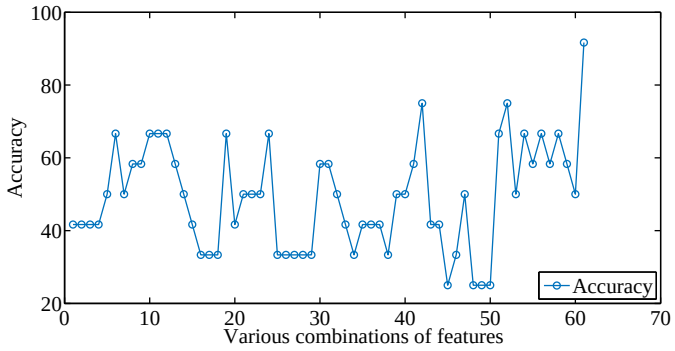

Figure 4.24 : Accuracy for various combinations of two features for classification of cage fault and outer-race faults using SVM2

Table 4.7 : Selected Features for SVM1

S.no.	Rank	Index	Feature	Time point	Frequency (Hz)
1.	1	2233	Std. deviation of magnitude	NA	17.5
2.	9	2455	Mean of Phase Angle	NA	150
3.	11	1036	Kurtosis of Magnitude	209	NA
4.	13	2337	Kurtosis of Magnitude	NA	142.5

Table 4.8 : Selected Features for SVM2

S.no.	Rank	Index	Feature	Time point	Frequency (Hz)
1.	6	2289	Kurtosis of Magnitude	56	NA
2.	7	1145	Maximum of Phase Angle	NA	30

combinations of two features in SVM2 are shown in Figure 4.24. The performances of both SVMs are summarized in Table 4.9.

Table 4.9 : Classification using SVM1 and SVM2

Class	Total Samples	Correctly Classified	Misclassified
SVM1			
#features = 4			
Ball Fault	6	6	0
Others	12	12	0
SVM2			
#features = 2			
Cage Fault	6	5	1
Outerrace Fault	6	6	0

Table 4.10 : Details of ANN

Layer	No. of Neurons	Transfer function	Accuracy
Input	6	linear	77.78%
Hidden layer	8	logsig	
Output layer	3	tansig	

The performance of the proposed method of classification is compared with that of ANN whose architecture is presented in Figure 4.25.The details of ANN are provided in Table 4.10.The selection of features fed to the ANN is carried out in the same way followed with SVM classifier.

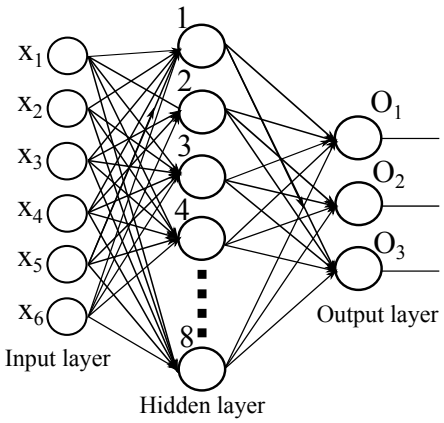

Figure 4.25 : Architecture of the ANN used

Table 4.11 : Selected Features for ANN

S.no.	Rank	Index	Feature	Time point	Frequency (Hz)
1.	2	5	FFT	NA	30
2.	4	2345	Maximum of Phase Angle	74	NA
3.	9	1265	Maximum of Phase Angle	NA	182.5
4.	10	1312	Maximum of Phase Angle	27	NA
5.	11	1229	Maximum of Phase Angle	110	NA
6.	12	2569	Std. dev. of Phase Angle	NA	22.5

The features as shown in Table 4.11 are fed as input to the ANN with 8 neurons in the hidden layer. ANN is trained to yield output $[O_1 O_2 O_3]$ as [1 0 0] for ball fault, [0 1 0] as cage fault and [0 0 1] as outer-race fault. The maximum efficiency achieved using ANN is found to be 77.78% which is less than the efficiency achieved with SVM classifier. The learning rate and momentum constant are chosen on trial and error basis.

The final algorithm for the detection, classification and locating the faulty bearings have been proposed using the following steps:
1. Fault detection is performed using the THD based method (Section 4.2.2).
2. Fault classification (Section 4.4).
3. Location of the faulty bearing is identified based on features from Stockwell transform (Section 4.3.2).

The performance of the algorithm has been established from the experimental data of defective bearings collected from the industry. The flow chart of the the proposed algorithm is shown in Figure 4.26. Table 4.12 presents the comparison of our proposed methodology with the existing literature. It is evident that the proposed methodology is more efficient with three number of faults.

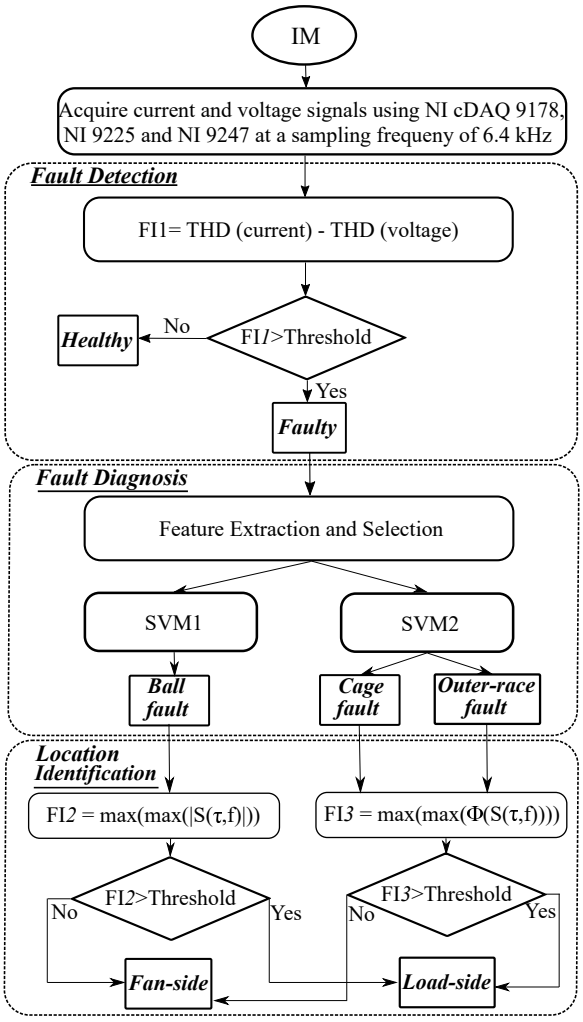

Figure 4.26 : Flowchart of the proposed algorithm

Table 4.12 : Comparison with the existing literature

Strategy	Data Source	References	Avg. Accuracy	Bearing Faults
FFT, SVM	Current	[Pandarakone et al., 2017]	96.67	2
Fourier Bessel, ARTMAP	Current	[Tran et al., 2013]	100	1
Discretized signal, SMO, kNN	Current	[Palácios et al., 2016]	90	3
WPD, ANN	Current	[Schmitt et al., 2015]	96.67	2
HHT,FFT-PCA	Vibration/Current	[Esfahani et al., 2014]	95	2
FFT,ANN/AFNIS	Vibration/Current	[Ertunc et al., 2013]	90-92	2
ST,SVM	**Current**	**Proposed work**	**95**	**3**

4.5 CONCLUSION

The final algorithm for the detection, classification and locating the faulty bearings have been proposed using the fault detection based on THD, fault classification using SVM and location of the faulty bearing is identified based on features from Stockwell transform. Because of simplicity of these independent algorithms, they are combined together to form a single algorithm. Thus,

detection, classification and location of faulty bearing in a three-phase induction motor is achieved by FFT and ST analysis of stator current signals with the help of SVM classifier. Fault detection is carried out by comparing a fault index with a predefined threshold which is computed based on THD of current and voltage signals. A set of features are selected from Stockwell Transform of current signals with the help of Fisher score ranking method and correlation techniques. These features are fed to SVM for the purpose of fault classification. Location of faulty bearing is achieved with the help of faulty indexes computed based on features extracted from ST. Hence, the proposed technique has been established with the experimental data obtained from the bearings collected from industry. Thus, it can be successfully utilized for online monitoring of bearing conditions and fault diagnosis of three-phase induction motor used in the industry. However, the proposed algorithm needs to be established for other faults such as inner race, spalling, brinelling etc. The feature selection in proposed algorithm is based on a minimum correlation of 50%, and can be verified for lower values as a part of future investigation.